



Phase-field modeling of switchable diode-like current-voltage characteristics in ferroelectric BaTiO₃

Y. Cao, J. Shen, C. A. Randall, and L. Q. Chen

Citation: [Applied Physics Letters](#) **104**, 182905 (2014); doi: 10.1063/1.4875902

View online: <http://dx.doi.org/10.1063/1.4875902>

View Table of Contents: <http://scitation.aip.org/content/aip/journal/apl/104/18?ver=pdfcov>

Published by the [AIP Publishing](#)

Articles you may be interested in

[High-rate performance of ferroelectric BaTiO₃-coated LiCoO₂ for Li-ion batteries](#)

Appl. Phys. Lett. **105**, 143904 (2014); 10.1063/1.4898006

[Interfacial dead layer effects on current-voltage characteristics in asymmetric ferroelectric tunnel junctions](#)

J. Appl. Phys. **113**, 174101 (2013); 10.1063/1.4803151

[Rectifying characteristic of perovskite oxide La_{1-x}Ce_xO₃/Ba_{0.5}Sr_{0.5}TiO₃/La_{0.67}Sr_{0.33}MnO₃ heterostructures](#)

J. Appl. Phys. **110**, 103716 (2011); 10.1063/1.3662909

[Intrinsic ferroelectric properties of the nonstoichiometric perovskite oxide Ba_{1-x}Ti_{1-y}O_{3-x-2y}](#)

J. Appl. Phys. **105**, 093519 (2009); 10.1063/1.3109210

[Ferroelectric domain wall relaxation in Ba_{0.25}Sr_{0.75}TiO₃ films displaying Curie-Weiss behavior](#)

J. Appl. Phys. **96**, 4392 (2004); 10.1063/1.1787587

AIP | Chaos

CALL FOR APPLICANTS
Seeking new Editor-in-Chief

Phase-field modeling of switchable diode-like current-voltage characteristics in ferroelectric BaTiO₃

Y. Cao,^{1,a)} J. Shen,² C. A. Randall,¹ and L. Q. Chen¹

¹Department of Materials Science and Engineering, The Pennsylvania State University, University Park, Pennsylvania 16802, USA

²Department of Mathematics, Purdue University, West Lafayette, Indiana 47907, USA

(Received 10 March 2014; accepted 21 April 2014; published online 7 May 2014)

A self-consistent model has been proposed to study the switchable current-voltage (I-V) characteristics in Cu/BaTiO₃/Cu sandwiched structure combining the phase-field model of ferroelectric domains and diffusion equations for ionic/electronic transport. The electrochemical transport equations and Ginzburg-Landau equations are solved using the Chebyshev collocation algorithm. We considered a single parallel plate capacitor configuration which consists of a single layer BaTiO₃ containing a single tetragonal domain orientated normal to the plate electrodes (Cu) and is subject to a sweep of ac bias from -1.0 to 1.0 V at 25°C . Our simulation clearly shows rectifying I-V response with rectification ratios amount to 10^2 . The diode characteristics are switchable with an even larger rectification ratio after the polarization direction is flipped. The effects of interfacial polarization charge, dopant concentration, and dielectric constant on current responses were investigated. The switchable I-V behavior is attributed to the polarization bound charges that modulate the bulk conduction. © 2014 AIP Publishing LLC. [<http://dx.doi.org/10.1063/1.4875902>]

Ferroelectric perovskites such as BaTiO₃ and BiFeO₃ have been extensively studied and widely used in various electronic applications.¹ The ferroelectric polarization has been recently found to affect the transport behavior in ferroelectrics.²⁻⁴ By controlling the polarization through external field, the charge transport is electrically tunable and unidirectional electric conduction can be realized. This rectifying current-voltage (I-V) characteristics enable ferroelectric perovskites potential device applications such as high resistance ratio diodes and electric resistive memory.⁵

The rectifying conduction characteristics were initially investigated by Blom *et al.* in Au/PbTiO₃/(LaSr)CoO₃ structure.⁶ Recent studies were mostly focused on the ferroelectric BiFeO₃ system.⁷⁻¹² Choi *et al.* reported a switchable diode-like I-V response associated with polarization flipping in mono-domain BiFeO₃ and attributed this behavior to the bulk conduction.⁷ Lee *et al.* suggested that the dominant space-charge-limited conduction mechanism and the modulation of interfacial carrier injection by polarization were responsible for the switchable diode effect in Pt/BiFeO₃/SrRuO₃ thin film capacitors.⁸ While it has long been demonstrated that the electromigration of oxygen vacancies towards cathode is an important ingredient for the resistance degradation behavior,¹³⁻¹⁷ Yi *et al.* recently showed that the ionic defect electromigration should also account for the switchable I-V characteristics in BiFeO₃.⁹ Wang *et al.* revealed that the polarization-modulated Schottky-like barriers at metal/ferroelectric interfaces result in the switchable rectifying behavior in the epitaxial BiFeO₃ thin film.¹⁰ Apart from experimental studies, Ge *et al.* proposed a numerical model and demonstrated that the switchable diode characteristics in BiFeO₃ capacitors could be explained by the polarization-modulated barrier, in agreement with Wang's experimental results.^{11,12} In spite of all these efforts, however,

most of them focused on BiFeO₃ system which has a high leaky current. It is unclear whether the switchable diode effect only exists in BiFeO₃ system or it is a general property for other ferroelectric materials. Although recent studies on large rectifying current-voltage behavior in BaTiO₃ capacitors were reported,¹⁸⁻²⁰ little consensus has been reached regarding whether the diode-like I-V response is originated from the bulk or interfacial conduction. To complement the experimental studies and fully understand the I-V behavior physics-based theoretical models and computational simulations capable of interplay between ferroelectric polarization and ionic/electronic conduction are of great demand.

In this work, we developed a phase-field model to understand the mechanism of switchable rectifying I-V characteristics in the presence of ionic/electronic transport and polarization bound charges in Cu/BaTiO₃/Cu ferroelectric capacitor. The phase-field approach has been extensively used to study the ferroelectric domain structures and domain switching²¹⁻²⁵ with ionic/electronic defects²⁶⁻²⁹ in both bulk and thin film perovskites. In the current model, we proposed to solve all the equations using spectral method based on Chebyshev transforms along the transport direction and Fourier transforms inside the plane which is normal to the transport direction.

In the phase-field simulation, the ferroelectric system can be represented by choosing the spontaneous polarization vector $P_i = (P_1, P_2, P_3)$ as the order parameter which describes the domain structure in ferroelectrics. The temporal evolution of the polarization in the system is modeled by numerically minimizing the total free energy of F with respect to polarization iteratively by solving the time-dependent Ginzburg-Landau (TDGL) equations²¹

$$\frac{\partial P_i(\mathbf{r}, t)}{\partial t} = -L \frac{\delta F}{\delta P_i(\mathbf{r}, t)}, \quad (i = 1, 2, 3), \quad (1)$$

^{a)}Electronic mail: ycx238@psu.edu

in which t is the time and L is the kinetic coefficient which is related to the domain evolution. The total free energy of the system F of BaTiO₃ single crystal is expressed as,²²

$$F = \int_V [f_{\text{lan}}(P_i) + f_{\text{grad}}(P_{i,j}) + f_{\text{elas}}(P_i, \varepsilon_{ij}) + f_{\text{elec}}(P_i, E_i)] dV, \quad (2)$$

where V is the system volume, ε_{ij} and E_i represent the components of strain and electric field, $f_{\text{lan}}(P_i)$, $f_{\text{grad}}(P_{i,j})$, $f_{\text{elas}}(P_i, \varepsilon_{ij})$, and $f_{\text{elec}}(P_i, E_i)$ are the Landau-Devonshire free energy density, the gradient energy density, elastic energy density, and the electrostatic energy density, respectively. Detailed expression of each of the local free energy densities can be found in Refs. 22–25.

The major ionic and electronic defects of interest in the system included the positively charged oxygen vacancies ($V_{\text{O}}^{\bullet\bullet}$) and holes (h^{\bullet}), and negatively charged electrons (e^{\prime}) and ionized acceptors (A^{\prime}) written in Kröger-Vink notation.³⁰ The monovalent acceptors were introduced from the substitution of trivalent Fe on the Ti sites ($\text{Fe}'_{\text{Ti}} = A^{\prime}$) and are considered as immobile under the applied fields. The electric field components, E_i , were found by solving the Poisson equation considering charges due to the ionic/electronic space charges and the gradients in the polarization components

$$-\nabla^2 \psi = \frac{\rho - \nabla \cdot P_i}{\varepsilon_0 \varepsilon_r} = \frac{e(2[V_{\text{O}}^{\bullet\bullet}] + p - n - [A^{\prime}]) - \nabla \cdot P_i}{\varepsilon_0 \varepsilon_r}, \quad (3)$$

in which ψ is the electric potential, ρ is the total space charges. ε_0 and ε_r are the vacuum permittivity and background dielectric constant of BaTiO₃. The electric field contribution to the dielectric constant has already been included in the Landau free energy density $f_{\text{lan}}(P_i)$ in Eq. (2). We used $\varepsilon_r = 44$ based on literature.³¹ $[V_{\text{O}}^{\bullet\bullet}]$, p , n , and $[A^{\prime}]$ denote the concentrations of oxygen vacancies, holes, electrons, and ionized acceptors, respectively. The electric field is related to the potential through $\vec{E} = -\nabla \psi$. The boundary condition of Eq. (3) is determined by

$$\psi|_{z=0} = V_a(0), \quad \psi|_{z=L} = V_a(L), \quad (4)$$

in which $V_a(0)$ and $V_a(L)$ are specified by the externally applied bias at $z = 0, L$.

The bulk transports of ionic/electronic defects are described by the diffusion equations. In the current simulation, only the oxygen vacancies, electrons, and holes are considered as mobile species. The oxygen vacancy transport is described by the classic Nernst-Planck transport model

$$J_{V_{\text{O}}^{\bullet\bullet}} = -D_{V_{\text{O}}^{\bullet\bullet}} \nabla [V_{\text{O}}^{\bullet\bullet}] + \mu_{V_{\text{O}}^{\bullet\bullet}} [V_{\text{O}}^{\bullet\bullet}] \vec{E}, \quad (5)$$

$$\frac{\partial [V_{\text{O}}^{\bullet\bullet}]}{\partial t} = -\nabla \cdot J_{V_{\text{O}}^{\bullet\bullet}} = D_{V_{\text{O}}^{\bullet\bullet}} \nabla^2 [V_{\text{O}}^{\bullet\bullet}] - \mu_{V_{\text{O}}^{\bullet\bullet}} \nabla \cdot [V_{\text{O}}^{\bullet\bullet}] \vec{E},$$

where $D_{V_{\text{O}}^{\bullet\bullet}}$ and $\mu_{V_{\text{O}}^{\bullet\bullet}}$ are the diffusivity and mobility of oxygen vacancy in BaTiO₃. $J_{V_{\text{O}}^{\bullet\bullet}}$ denotes the flux of oxygen vacancies. The Cu electrodes act as the blocking boundary for oxygen vacancy transport, i.e., there will be no $V_{\text{O}}^{\bullet\bullet}$ transfer between the ferroelectrics and the electrodes and the total

amount of oxygen vacancy is conserved. Therefore, the boundary condition for oxygen vacancy transport equation is given by

$$J_{V_{\text{O}}^{\bullet\bullet}}|_{z=0,L} = 0. \quad (6)$$

On the other hand, electrons and holes move much faster than oxygen vacancies due to higher mobility. We assume that electrons and holes reach steady state for each evolution of oxygen vacancy. Mathematically, we solve steady state equations for electron and hole transports assuming $\partial n / \partial t = 0$ and $\partial p / \partial t = 0$

$$\frac{\partial n}{\partial t} = -\nabla \cdot J_n = D_n \nabla^2 n + \mu_n \nabla \cdot [n \vec{E}] = 0, \quad (7)$$

$$\frac{\partial p}{\partial t} = -\nabla \cdot J_p = D_p \nabla^2 p - \mu_p \nabla \cdot [p \vec{E}] = 0.$$

We assume that the electron and hole concentrations at the Cu/BaTiO₃ interfaces are pinned by the Cu electrodes. The boundary conditions of electronic transports are specified as

$$n_{z=0,L} = N_c \exp\left(-\frac{E_c - E_{fm}}{k_B T}\right), \quad (8)$$

$$p_{z=0,L} = N_v \exp\left(-\frac{E_{fm} - E_v}{k_B T}\right),$$

in which N_c and N_v are the effective density of states in the conduction and valence band of BaTiO₃, where E_c and E_v represent the energy of the conduction band minimum and valence band maximum. E_{fm} is the work function of Cu plate electrode, and k_B is the Boltzmann constant.

The local current due to the mobile space charges and the total current are calculated as

$$I(z) = \sum_i e_0 z_i J_i(z), \quad i = V_{\text{O}}^{\bullet\bullet}, e^{\prime}, p^{\bullet}, \quad (9)$$

$$\frac{1}{I_{\text{total}}} = \frac{1}{n} \sum_z \frac{1}{I(z)},$$

in which z_i and J_i denote the charge number and the flux of each charge species, $I(z)$ is the local current density at position z , I_{total} is the overall current density, and n is the number of grid points along z .

We considered at first an ideal model of single crystal BaTiO₃ ($L = 300$ nm) of a single tetragonal domain oriented to the normal of the Cu electrode plates in a single layer capacitor configuration (Fig. 1(a)). Periodic boundary conditions were applied along x and y directions and non-periodic boundary condition along the longitudinal z direction. The ferroelectric polarization, the applied field, and the charge transport were assumed to be along z direction. A one-dimensional simulation size of $1 \times 1 \times 200$ was chosen for the simulation. The temporal evolution of the polarization field and the defect concentrations were obtained by numerically solving the TDGL and diffusion equations using the semi-implicit Fourier spectral method.^{32–35} The appropriate material constants of BaTiO₃ for the Landau thermodynamic polynomial, with the polarization coupling to the electrostrictive effect, electric

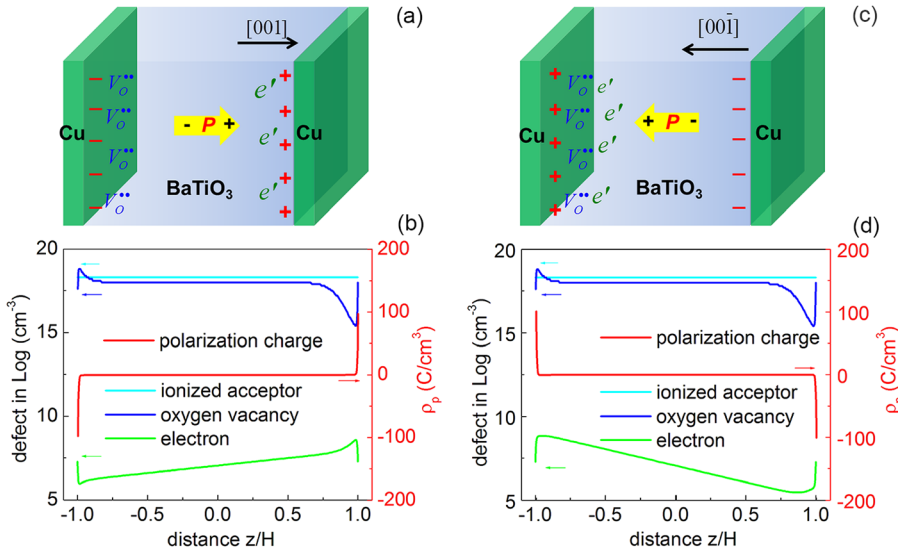


FIG. 1. Schematic [(a) and (c)] and calculated [(b) and (d)] equilibrium profiles of the metal (Cu)/ferroelectric (BaTiO₃)/metal (Cu) sandwiched configuration with [001] [(a) and (b)] and [00 $\bar{1}$] [(c) and (d)] oriented polarization, polarization induced charges and ionic/electronic space charges under room temperature ($T = 25^\circ\text{C}$). The + and - signs in (a) and (c) represent the polarization induced interfacial charges. V_O^{**} and e' denote the major ionic and electronic space charges. $H = 150\text{ nm}$ is half of the layer thickness, so that z/H from -1 to $+1$ represents the entire BaTiO₃ single layer.

properties, and elastic properties required for expressing the system energy in Eq. (2) were collected from literature.³⁶ Other parameters used in the simulation are listed in Table I.

The acceptor dopant concentration was chosen to be $2.0 \times 10^{18}\text{ cm}^{-3}$. All the ionic/electronic defects were assumed to be homogeneous in the initial state and the local charge neutrality condition was maintained

$$2[V_O^{**}] + p - n - [A'] = 0. \quad (10)$$

The initial polarization inside bulk BaTiO₃ was assumed to be along [001] direction ($P > 0$), and equal to the spontaneous polarization $P = P_s = 26\mu\text{C}/\text{cm}^2$. At the Cu/BaTiO₃ interfaces, the polarization boundary condition in 1D was specified as

$$a \times P_z - b \times \frac{dP_z}{dz} \Big|_{z=0} = 0, \quad a \times P_z + b \times \frac{dP_z}{dz} \Big|_{z=L} = 0, \quad (11)$$

where coefficients a and b were chosen to be 1.0 and 0.0135 cm representing a partially compensated boundary condition.

The schematic and calculated polarization induced bound charges (ρ_p) at metal/ferroelectric interfaces and ionic/electronic defect concentrations at equilibrium state were presented in Figs. 1(a) and 1(b). The [001] oriented ferroelectric polarization resulted in net positive charges at $z/H = +1$ and negative charges at $z/H = -1$ (red line in Fig. 1(b)). Consequently, oxygen vacancies and electrons segregated at $z/H = -1$ and $z/H = +1$, respectively, for charge compensation. The concentration of holes was much lower

TABLE I. Parameters for the simulation.

Parameter	Value	Parameter	Value
T (K)	298	E_c (eV)	-3.6
L (nm)	300	E_v (eV)	-6.7
ϵ_r	44	E_{fm} (eV)	-4.5
$\mu_{V_O^{**}}$ ($\text{cm}^2\text{ V}^{-1}\text{ s}^{-1}$)	10^{-14}	N_c, N_v (cm^{-3})	10^{22}

than oxygen vacancies and electrons and was negligible. The acceptor was immobile and remained constant in the entire BaTiO₃ layer. It should be noted that the polarization induced bound charges were not fully screened by the space charges. This agrees with recent publication.³⁷

When equilibrium state was reached, the forward ($V > 0$) and reverse biases ($V < 0$) were applied and swept from -1.0 V to $+1.0\text{ V}$. We assumed that the sweeping rate was fast enough, and the applied field was much smaller than the coercive field so that neither oxygen vacancies migration nor polarization switching occurred. Therefore, the total current was mainly contributed from electronic defects of high mobility. Fig. 2 clearly shows a pronounced I-V response under forward bias and suppressed response under reverse bias (red line). The log (I)-V plot in the inset of Fig. 2 (red line) indicates that the rectification ratio at maximum biases amounts to $r = |I(+1\text{V})/I(-1\text{V})| \approx 120$. A possible explanation for this nonlinear I-V behavior is that the polarization promotes the defect transport when the capacitor is under forward bias and inhibits the transport when it is under reverse bias. To verify this, we studied the spatial evolution of electrons under external bias as shown in Fig. 3. In the vicinity of cathode ($z/H = +1$), the electrons

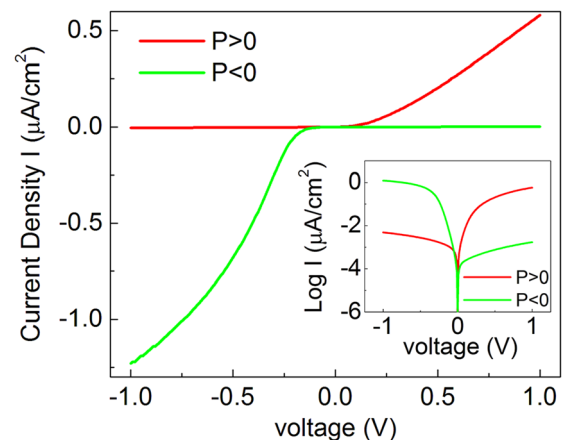


FIG. 2. I-V response in Cu/BaTiO₃/Cu capacitor subject to ac bias (-1.0 V to $+1.0\text{ V}$) at $T = 25^\circ\text{C}$ before ($P > 0$) and after polarization switching ($P < 0$).

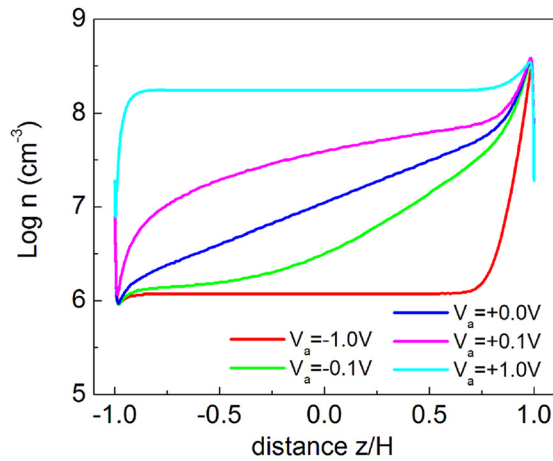


FIG. 3. Electronic evolution in BaTiO₃ under biases (-1.0 V to $+1.0$ V) with $[001]$ oriented polarization.

segregated under both forward and reverse bias. This is due to the charge compensation to the positive polarization charges in this region. However, inside the bulk BaTiO₃ layer the electron concentration significantly increased under forward bias and decreased under reverse bias, the difference of which reached more than 10^2 at ± 1.0 V. The electron evolution clearly explained the asymmetric current-voltage response and agreed well with the calculated rectification ratio at ± 1.0 V.

In order to further understand the effect of polarization on the I-V behavior, we poled the $[001]$ oriented BaTiO₃ into an $[00\bar{1}]$ oriented single domain by applying a -10 V pulse. The schematic and calculated polarization induced interfacial charges and defect distributions were shown in Figs. 1(c) and 1(d). Due to the switched locations of positive/negative polarization charges after the polarization flip, the electrons tended to segregate at $z/H = -1$ and deplete at $z/H = +1$. The oxygen vacancies were assumed immobile during the polarization switching due to its extremely low mobility. The I-V measurement on BaTiO₃ with reversed polarization showed similar I-V behavior (green line in Fig. 2) with enhanced current response under forward bias ($V < 0$) and inhibited response under reverse bias ($V > 0$). However, the rectification ratio at ± 1.0 V of switched BaTiO₃ amounts to 720. This can be explained by the extra interfacial space charges ascribed to the immobile oxygen vacancies during polarization switching, causing even larger electronic segregation/depletion at the interfaces (green line in Fig. 1(d)).

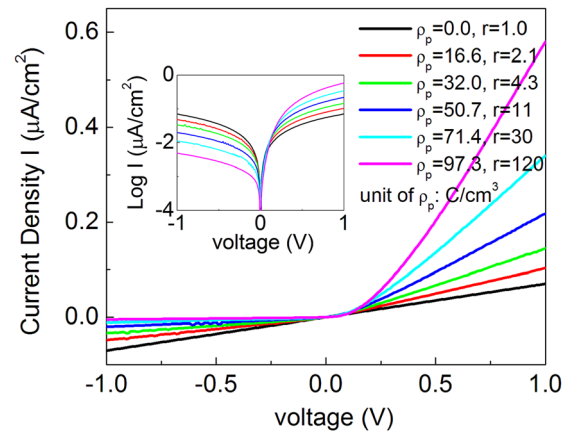


FIG. 4. I-V curve evolution with different polarization induced interfacial charges.

The effect of dopant concentration, extent of electronic screening, and the uncompensated interfacial polarization charge condition on the current-voltage response were studied and presented in Figures 4 and 5. The amount of uncompensated polarization interfacial charges (ρ_p) is tunable by changing the b/a ratios in Eq. (11). The dopant (acceptor) concentration $[A']$ and the dielectric constant ϵ_r were fixed to be $2.0 \times 10^{18} \text{ cm}^{-3}$ and 44, respectively, while the polarization charges changed from 0.0 to 97.34 C/cm^3 . Fig. 4 illustrates the dependence of I-V behavior on polarization charges, in which I-V behavior undergoes from ohmic-like relation to diode-like characteristics with increasing polarization interfacial charges, and the rectification ratios increase from 1.0 to 120. This could be understood since the increasing amount of uncompensated polarization charges induces more compensating ionic and electronic carriers, resulting in larger electronic current under biases. Fig. 5(a) and the inset show that both segregated electron concentrations ($\text{Log } n$) at cathode and the current response ($\text{Log } I$) at 1.0 V exhibit exponential dependence on $\text{Log } (\rho_p)$ (black line) and the slope increases from 0.5 to 1.7 obtained from the $d(\text{Log } I)/d(\text{Log } \rho_p)$ vs. $\text{Log } (\rho_p)$ plot (red line). This indicates that the enhanced current response is attributed to the polarization-modulated electronic conduction.

To study the effect of dopant (acceptor) concentration $[A']$ on current response, we chose a series of concentrations $[A']$ from 10^{16} cm^{-3} to 10^{19} cm^{-3} . The polarization interfacial charges $\rho_p = 97.34 \text{ C/cm}^3$ and dielectric constant $\epsilon_r = 44$ were fixed for different $[A']$. From Figure 5(b), the current

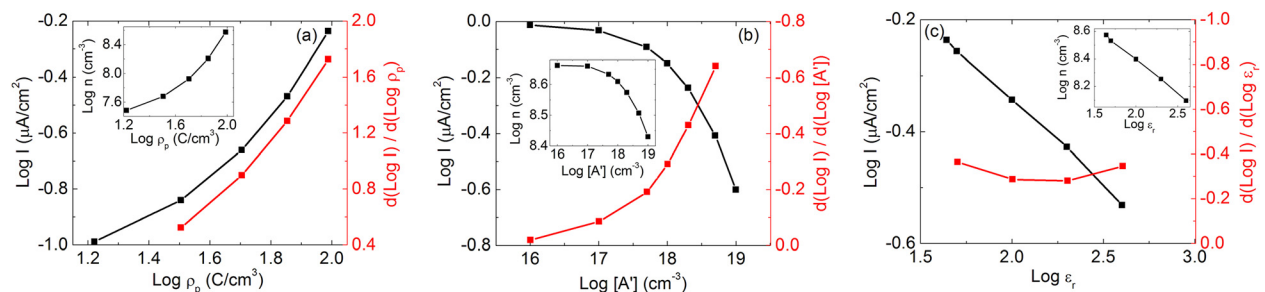


FIG. 5. Dependence of current response at 1.0 V bias and electron segregated concentration at $z=L$ on: (a) polarization charges ρ_p , (b) dopant concentration $[A']$, and (c) dielectric constant ϵ_r .

density becomes almost constant when $[A']$ is lower than 10^{17}cm^{-3} and decreases significantly with increasing $[A']$. This could be explained by the fact that the increasing dopant concentration results in more oxygen vacancies with both dopants and oxygen vacancies compensating the polarization induced interfacial charges. The increasing ionic defects reduce the segregation and depletion of compensating electronic carriers at interfaces with a fixed ρ_p . This argument is supported by the $\text{Log } n$ vs. $\text{Log } [A']$ plot as shown in Fig. 5(b) inset. Since electronic currents are 3–4 orders of magnitude higher than ionic currents, the diminishing interfacial electrons lead to decreasing total currents at maximum biases. A replot of $d(\text{Log } I)/d(\text{Log } [A'])$ vs. $\text{Log}[A']$ indicates that the current density is more sensitive to $[A']$ at large $[A']$ than at small $[A']$, with slope from ~ -0.01 at $[A'] = 10^{16}\text{cm}^{-3}$ to ~ -0.6 at $[A'] = 10^{19}\text{cm}^{-3}$ (red line in Fig. 5(b)). By comparing Figs. 5(a) and 5(b), it was observed that the current response to dopant concentration is smaller than to the polarization induced interfacial charges.

Finally, the effect of dielectric constant on the current response was studied and presented in Fig. 5(c). We chose ϵ_r from 44 to 400. It was found out that both electronic segregation ($\text{Log } n$) and the current response ($\text{Log } I$) exhibit linear dependence on $\text{Log } (\epsilon_r)$; the slope of the latter was calculated to be -0.32 in average from the $d(\text{Log } I)/d(\text{Log } (\epsilon_r))$ vs. $\text{Log } (\epsilon_r)$ plot. This is due to the fact that the electric potential increases with decreasing ϵ_r at fixed polarization charges based on Eq. (3), resulting in an exponential enhancement of electronic concentration (from Boltzmann approximation) and electronic current. Therefore, the extent of electronic screening to the polarization charges can be effectively modulated by tuning the dielectric constant.

In summary, we developed a phase-field model to study the current-voltage characteristics in single crystal BaTiO_3 of single tetragonal domain which takes into account the interplay between ferroelectric polarization and ionic/electronic transport. Our model demonstrates diode-like I-V responses which are dependent on the ferroelectric polarization and shows the switchable diode polarity by reversing the polarization direction. The rectification ratios reach up to 10^2 which are consistent with recent experimental measurements. The current response decreases with decreasing uncompensated polarization charges, with increasing dopant concentrations and dielectric constant. The non-linear I-V behavior can be attributed to the polarization bound charges which modulate the electronic bulk conduction inside BaTiO_3 single layer.

The authors are grateful to the financial support for NSF-IUCRC Center for Dielectric Studies at Pennsylvania State (Cao and Randall) and by the U.S. Department of Energy, Office of Basic Energy Sciences, Division of Materials Sciences and Engineering under Award No. DE-FG02-07ER46417 (Chen). The work at Purdue was partially supported by NSF DMS-1215066 and by the

Computational Materials and Chemical Sciences Network (CMCSN)

- ¹O. Auciello, J. F. Scott, and R. Ramesh, *Phys. Today* **51**(7), 22 (1998).
- ²C. H. Yang, J. Seidel, S. Y. Kim, P. B. Rossen, P. Yu, M. Gajek, Y. H. Chu, L. W. Martin, M. B. Holcomb, Q. He, P. Maksymovych, N. Balke, S. V. Kalinin, A. P. Baddorf, S. R. Basu, M. L. Scullin, and R. Ramesh, *Nature Mater.* **8**, 485 (2009).
- ³L. Pintilie, I. Boerasu, M. J. M. Gomes, T. Zhao, R. Ramesh, and M. Alexe, *J. Appl. Phys.* **98**, 124104 (2005).
- ⁴V. Garcia, S. Fusil, K. Bouzehouane, S. Enouz-Vedrenne, N. D. Mathur, A. Barthelemy, and M. Bibes, *Nature* **460**, 81 (2009).
- ⁵A. Gruverman, D. Wu, H. Lu, Y. Wang, H. W. Jang, C. M. Folkman, M. Y. Zhuravlev, D. Felker, M. Rzechowski, C. B. Eom, and E. Y. Tsymbal, *Nano Lett.* **9**, 3539 (2009).
- ⁶P. W. M. Blom, R. M. Wolf, J. F. M. Cillessen, and M. P. C. M. Krijn, *Phys. Rev. Lett.* **73**, 2107 (1994).
- ⁷T. Choi, S. Lee, Y. J. Choi, V. Kiryukhin, and S. W. Cheong, *Science* **324**, 63 (2009).
- ⁸D. Lee, S. H. Baek, T. H. Kim, J. G. Yoon, C. M. Folkman, C. B. Eom, and T. W. Noh, *Phys. Rev. B* **84**, 125305 (2011).
- ⁹H. T. Yi, T. Choi, S. G. Choi, Y. S. Oh, and S. W. Cheong, *Adv. Mater.* **23**, 3403 (2011).
- ¹⁰C. Wang, K. J. Jin, Z. T. Xu, L. Wang, C. Ge, H. B. Lu, H. Z. Guo, M. He, and G. Z. Yang, *Appl. Phys. Lett.* **98**, 192901 (2011).
- ¹¹C. Ge, K. J. Jin, C. Wang, H. B. Lu, C. Wang, and G. Z. Yang, *Appl. Phys. Lett.* **99**, 063509 (2011).
- ¹²C. Ge, K. J. Jin, C. Wang, H. B. Lu, C. Wang, and G. Z. Yang, *J. Appl. Phys.* **111**, 054104 (2012).
- ¹³G. Y. Yang, E. C. Dickey, C. A. Randall, M. S. Randall, and L. A. Mann, *J. Appl. Phys.* **94**, 5990 (2003).
- ¹⁴G. Y. Yang, G. D. Lian, E. C. Dickey, C. A. Randall, D. E. Barber, P. Pinceloup, M. A. Henderson, R. A. Hill, J. J. Beeson, and D. J. Skamser, *J. Appl. Phys.* **96**, 7500 (2004).
- ¹⁵R. M. Waser, *J. Am. Ceram. Soc.* **72**, 2234 (1989).
- ¹⁶H. Chazono and H. Kishi, *Jpn. J. Appl. Phys., Part 1* **40**, 5624 (2001).
- ¹⁷H. Kishi, Y. Mizuno, and H. Chazono, *Jpn. J. Appl. Phys., Part 1* **42**, 1 (2003).
- ¹⁸C. J. Won, Y. A. Park, K. D. Lee, H. Y. Ryu, and N. Hur, *J. Appl. Phys.* **109**, 084108 (2011).
- ¹⁹T. J. Zhang, R. K. Pan, Z. J. Ma, M. G. Duan, D. F. Wang, and M. He, *Appl. Phys. Lett.* **99**, 182106 (2011).
- ²⁰R. K. Pan, T. J. Zhang, J. Z. Wang, Z. J. Ma, J. Y. Wang, and D. F. Wang, *J. Alloys Compd.* **519**, 140 (2012).
- ²¹H. L. Hu and L. Q. Chen, *Mater. Sci. Eng., A* **238**, 182 (1997).
- ²²Y. L. Li, S. Y. Hu, Z. K. Liu, and L. Q. Chen, *Appl. Phys. Lett.* **78**, 3878 (2001).
- ²³Y. L. Li, L. E. Cross, and L. Q. Chen, *J. Appl. Phys.* **98**, 064101 (2005).
- ²⁴Y. L. Li, S. Y. Hu, Z. K. Liu, and L. Q. Chen, *Acta Mater.* **50**, 395 (2002).
- ²⁵Y. L. Li, L. Q. Chen, G. Asayama, D. G. Schlom, M. A. Zurbuchen, and S. K. Streiffer, *J. Appl. Phys.* **95**, 6332 (2004).
- ²⁶P. Suryanarayana and K. Bhattacharya, *J. Appl. Phys.* **111**, 034109 (2012).
- ²⁷Y. Xiao and K. Bhattacharya, *Proc. SPIE* **5387**, 354 (2004).
- ²⁸Y. Xiao, V. B. Shenoy, and K. Bhattacharya, *Phys. Rev. Lett.* **95**, 247603 (2005).
- ²⁹Y. Xiao and K. Bhattacharya, *Arch. Ration. Mech. Anal.* **189**, 59 (2008).
- ³⁰F. A. Kroger and H. J. Vink, *Solid State Phys. - Adv. Res. Appl.* **3**, 307 (1956).
- ³¹G. Rupprecht and R. O. Bell, *Phys. Rev. A* **135**, A748 (1964).
- ³²L. Q. Chen and J. Shen, *Comput. Phys. Commun.* **108**, 147 (1998).
- ³³J. Shen and T. Tang, *Spectral and High-Order Methods with Applications* (Chinese Science Press, Beijing, China, 2006).
- ³⁴J. Shen, T. Tang, and L. L. Wang, *Spectral Methods: Algorithms, Analysis and Applications* (Springer, 2011).
- ³⁵Y. Cao, S. Bhattacharya, J. Shen, C. A. Randall, and L. Q. Chen, *J. Appl. Phys.* **114**, 224102 (2013).
- ³⁶G. Sheng, J. X. Zhang, Y. L. Li, S. Choudhury, Q. X. Jia, Z. K. Liu, and L. Q. Chen, *Appl. Phys. Lett.* **93**, 232904 (2008).
- ³⁷T. Sluka, A. K. Tagantsev, D. Damjanovic, M. Gureev, and N. Setter, *Nature Commun.* **3**, 748 (2012).